J. Fluid Mech. (1991), *vol.* 229, *pp.* 159–171
Printed in Great Britain

Viscous forces on a circular cylinder in orbital flow at low Keulegan–Carpenter numbers

By P. K. STANSBY[1] AND P. A. SMITH[2]

[1] Department of Engineering, Simon Building, The University, Manchester M13 9PL, UK
[2] Paul Scherrer Institute, Wurenlingen, CH-5232 Villigen PSI, Switzerland

(Received 30 March 1990 and in revised form 1 October 1990)

The flow structures giving rise to the force on a circular cylinder in uniform, circular, orbital flows have been investigated for Keulegan–Carpenter numbers (K) less than 2 and a Stokes parameter (β) of 483 using the random-vortex method. Comparisons with analysis using the method of inner and outer expansions are made and good agreement is found for $K = 0.1$. For higher K-values, the viscous force (the difference between the total force and the potential-flow force) acts mainly in opposition to the potential-flow force causing a substantial reduction in total force, in keeping with experimental measurements. Significant separation does not occur at $K \leqslant 1.5$ and vorticity organizes itself asymmetrically about the line through the cylinder centre parallel to the incident velocity vector. Vorticity of one sense of rotation remains close to the half-surface lagging the velocity vector, while an area of vorticity of the opposite sense wraps itself around the cylinder. The net circulation in the flow (the circulation within a path encircling the cylinder at a large radius) is zero. Vortex shedding occurs at $K > 1.5$. Viscous forces due to non-uniform, orbital flows around a horizontal cylinder beneath waves were similar although vortex shedding tended to occur at lower K-values.

1. Introduction

Uniform orbital flow is defined here as one where the motion of fluid elements describe closed paths. Such a flow around a circular cylinder may be characterized by the Keulegan–Carpenter number, K, the Stokes parameter, β, and the geometry of the particle path in the onset flow (circular or elliptical in this study):

$$K = UT/2a$$

and

$$\beta = 4a^2/\nu T,$$

where U is the amplitude of the horizontal component of onset velocity, T is the orbital period, a is the cylinder radius and ν is the kinematic viscosity. Here, we limit ourselves to K-values below 2, for which vortex shedding is not, in the main, a significant effect.

The practical concern in the field of offshore engineering is to understand the flow mechanisms which generate viscous forces on a horizontal cylinder under regular waves, where the cylinder axis is parallel to the wave crests and submerged at a depth great enough not to modify the surface wave form. Under waves, the orbital flow is non-uniform and may be defined by two non-dimensional parameters in addition to K and β, provided linear wave theory is valid: the ratio of the depth of

the cylinder centre beneath mean water level to the cylinder radius, and the depth parameter ($2\pi \times$ water depth/wavelength). Comparisons with uniform orbital flow, having the same onset velocities at the cylinder centre, will be made.

In linear, oscillatory, onset flow at K below about 2, the force on a circular cylinder is close to the potential flow, inertia force for a wide range of β-values spanning laminar and turbulent conditions; the viscous force is relatively small and, in laminar conditions, is predicted reasonably by the analyses of Stokes (1951) and Wang (1968), see, for example, Bearman *et al.* (1985) and Sarpkaya (1986). The vorticity structures associated with laminar flow have recently been investigated computationally by Smith & Stansby (1991). Experimental measurements of the force on a horizontal cylinder under deep-water waves (at β-values where turbulent or transitional flow would be expected) have, on the other hand, shown that the force is substantially modified from the potential-flow force for the same range of K-values (Chaplin 1984*b*). The inertia coefficient for total force, defined in the conventional way, decreases as K increases, indicating that a component of the viscous force acts in opposition to the potential-flow force. However, for laminar conditions, the analysis of Riley (1971) for uniform, circular, orbital flow predicts a viscous force component in the direction of the potential-flow force, giving an increased inertia coefficient for total force. In this analysis (and that of Wang) the flow is divided into an inner boundary-layer region and an outer region, with separate expansions of the stream function which match asymptotically. Steady streaming is predicted and this drift of fluid elements around the surface, with the same sense of rotation as the onset orbital flow, has also been observed in the experiments with waves (Chaplin 1984*a*). Chaplin (1984*b*) has postulated that the 'bound circulation' associated with the steady streaming in Riley's analysis gives rise to a force proportional to U^3. Since the terms in the expansions from this analysis do not extend to this order, steady streaming makes no contribution to the forces derived. The force vector associated with a bound circulation would lag the velocity vector by $\frac{1}{2}\pi$ and act in opposition to the potential-flow force, since the acceleration vector leads the velocity vector by $\frac{1}{2}\pi$ (see the definition sketch in figure 1). Chaplin (1984*b*) has thus inferred that the reduction in the inertia coefficient for total force with increasing K is associated with this bound circulation. Clearly the situation is rather different from that with linear, oscillatory, onset flow.

To improve understanding of the flow structures generating the viscous forces, we solve the starting-flow problem numerically using the random-vortex method for two-dimensional, laminar flow. At zero time there is no vorticity in the flow and, in general, the time-stepping computation is continued until steady periodic motion at least appears to have been reached. In this way the evolution of the flow structures may be observed. With this method, point vortices are generated around the surface at each time step to satisfy the zero-slip condition and maintain a constant circulation thereafter. Vortices are convected by the vortex-in-cell method and diffusion is simulated using random walks at each time step. The local rate of generation of circulation on the surface may be shown to be proportional to the tangential pressure gradient, requiring the rate of generation of circulation around a complete surface to be zero. The net circulation in the flow is thus zero. Since this result is particularly relevant to this problem its derivation will be given in full in this paper. The net circulation in the flow has also been shown to be zero through purely kinematical considerations (Milne-Thomson 1968).

The transport of vortical regions is a vital aspect of this flow and it can be represented accurately by the random-vortex method, avoiding some of the

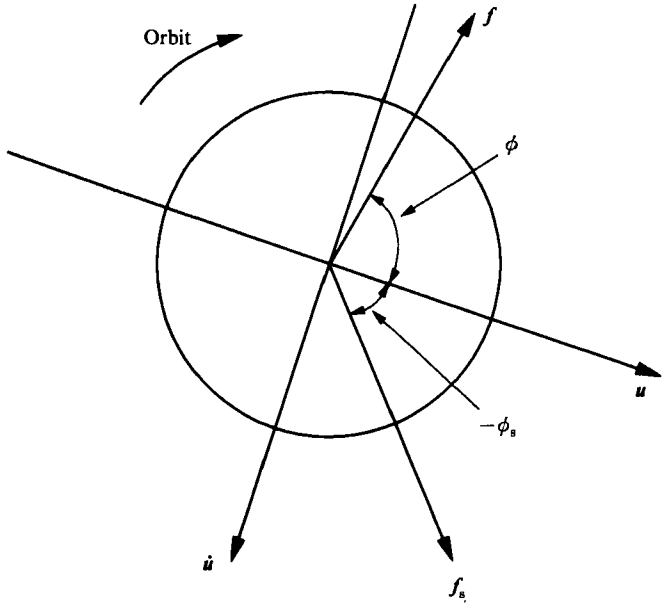

FIGURE 1. Definition sketch, showing the viscous force vector $\boldsymbol{f}$, shear force vector $\boldsymbol{f}_s$, velocity vector $\boldsymbol{u}$, acceleration $\dot{\boldsymbol{u}}$ and relative phase angles ϕ and ϕ_s. The velocity vector lags the acceleration vector by $\frac{1}{2}\pi$ only when the orbital flow is circular.

numerical diffusion and dissipation problems associated with Eulerian, finite-difference schemes. The method thus appears to be well suited to this problem. The formulation used here is the same as that in Smith & Stansby (1988, 1989), with different boundary conditions for the onset flow.

A direct comparison with experimental data is, however, not possible since the minimum β-value in the experiments was 7600 and these orbital flows will almost certainly be three-dimensional and turbulent for most of the K-range. Since our numerical solution requires two-dimensional, laminar flow, we set $\beta = 483$, a situation which has been investigated experimentally for linear, oscillatory, onset flow (Bearman *et al.* 1985). With $K \leqslant 1.5$, flows have been found to be two-dimensional. Some results with $\beta = 100$ have also been computed. As direct, three-dimensional simulation is not yet achievable, we are limited to such an indirect route to improve understanding of flows which are difficult to analyse through physical experiment.

We are concerned here with viscous forces. The viscous force is considered in relation to the incident velocity vector and the component due to shear stress is an output as well as the total viscous force. Streamline plots with superimposed areas of vorticity of different rotation are produced at regular time intervals.

2. Theory

The theory and numerical formulation for the random-vortex method have been given in Smith & Stansby (1988, 1989) and only an outline will be given here. In two dimensions, viscous flow of an incompressible fluid with constant kinematic viscosity is described by two coupled partial differential equations: the vorticity equation

$$\frac{\partial \omega}{\partial t} = -(\boldsymbol{u}\cdot\nabla)\,\omega + \nu\nabla^2\omega, \tag{1}$$

and a Poisson equation

$$\nabla^2 \boldsymbol{u} = -\nabla \wedge (\omega \boldsymbol{k}), \tag{2}$$

where ω is the magnitude of vorticity, $\boldsymbol{u}$ is the velocity, t is time and $\boldsymbol{k}$ is a unit vector normal to the plane of the flow. Equation (1) is solved by the operator-splitting scheme of Chorin (1973). The equation is separated into the nonlinear Euler equation

$$\left[\frac{\partial \omega}{\partial t}\right]_{\mathrm{C}} = -(\boldsymbol{u}\cdot\nabla)\,\omega \tag{3}$$

and the linear diffusion equation

$$\left[\frac{\partial \omega}{\partial t}\right]_{\mathrm{D}} = \nu \nabla^2 \omega. \tag{4}$$

The processes of convection and diffusion are denoted by the suffices C and D respectively. The time-stepping procedure by which these equations are to be solved is the random-vortex method. The vorticity field is represented by a field of point vortices. New vortices are created around the cylinder surface at each time step. A circulation is associated with each new vortex such that the zero-slip condition is satisfied. Equation (3) is solved by convecting vortex particles in their mutually induced velocity field, obtained from (2) by the vortex-in-cell method, using a radially expanding polar mesh. Equation (4) is solved by superimposing normally distributed random walks onto the positions of the vortex particles.

In order to maintain the zero-slip condition throughout one time step, vortex particles which are carried across the surface by the random walk may be reflected back to their mirror-image positions (Chorin 1978). Alternatively these particles may be 'absorbed' and the circulation carried by the newly created vortices adjusted so that the zero-slip generation condition is still satisfied (Smith & Stansby 1989). This has the advantage of substantially reducing the number of vortices which are needed for convergence of flow properties.

The kinematics on the outer boundary of the vortex-in-cell mesh are imposed using either linear wave theory or a uniform orbital flow. Varying the position of this boundary from 20 to 40 radii from the cylinder centre had negligible effect on the results computed.

3. Surface conditions and net circulation

In Smith & Stansby (1988) the relation between surface pressure and the circulation carried by vortices generated on the surface was stated, following the derivation given in Smith (1986). This is now given in a concise form.

Close to the surface of the cylinder, convective transport may be neglected, so that transport of vorticity is described by the diffusion equation (4) with $\partial\omega/\partial t \approx [\partial\omega/\partial t]_{\mathrm{D}}$. This can be rewritten in terms of vorticity flux vector $\boldsymbol{\gamma}$ as

$$\frac{\partial \omega}{\partial t} = -\nabla\cdot\boldsymbol{\gamma}, \tag{5}$$

where

$$\boldsymbol{\gamma} = -\nu\nabla\omega. \tag{6}$$

The surface is divided into N small elements of arclength $\Delta\theta$ ($\Delta\theta = 2\pi/N$). We denote the radial component of $\boldsymbol{\gamma}$ at a point on the cylinder surface situated within the ith

surface element by $(1/a\Delta\theta)\partial(\Delta\Gamma_i)/\partial t$. Thus $\partial(\Delta\Gamma_i)/\partial t$ approximates the rate at which circulation crosses the surface element:

$$\frac{\partial}{\partial t}(\Delta\Gamma_i) = -\nu a\,\Delta\theta \left.\frac{\partial\omega}{\partial r}\right|_{\theta=i\Delta\theta}. \tag{7}$$

Transport of momentum is described by the Navier–Stokes equations. Again neglecting convective transport close to the cylinder surface, we obtain

$$\begin{aligned}\frac{\nabla p}{\rho} &= \nu\nabla^2\boldsymbol{u} \\ &= \nu[\nabla(\nabla\cdot\boldsymbol{u}) - \nabla\wedge(\nabla\wedge\boldsymbol{u})];\end{aligned} \tag{8}$$

$\omega \equiv -\nabla\wedge\boldsymbol{u}$ and, in incompressible flow, $\nabla\cdot\boldsymbol{u} = 0$. Hence

$$\frac{\nabla p}{\rho} = \nu\nabla\wedge\boldsymbol{\omega}. \tag{9}$$

Integrating the tangential component of (9) along the ith surface element, we obtain

$$\Delta p_i = -\rho\nu a\,\Delta\theta \left.\frac{\partial\omega}{\partial r}\right|_{\theta=i\Delta\theta}, \tag{10}$$

where Δp_i is the pressure change along the element. From (7) and (10)

$$\Delta p_i = \rho\frac{\partial}{\partial t}(\Delta\Gamma_i). \tag{11}$$

We define $\delta\Gamma_i$ by

$$\delta\Gamma_i = \frac{\partial}{\partial t}(\Delta\Gamma_i)\,\Delta t; \tag{12}$$

$\delta\Gamma_i$ then represents the circulation carried by vortices crossing the ith surface element in a time increment Δt. The pressure p_i at $\theta = i\Delta\theta$, relative to a reference pressure p_0 at $\theta = 0$, is given by

$$p_i = p_0 + \frac{\rho}{\Delta t}\sum_{j=1}^{i}\delta\Gamma_j. \tag{13}$$

Since the surface pressure can contain no discontinuities, $p_N = p_0$ and

$$\sum_{j=1}^{N}\delta\Gamma_j = 0. \tag{14}$$

Thus the sum of the circulation is carried by vortices crossing the cylinder surface, and the net circulation remains zero, which is consistent with the kinematical result given in Milne-Thomson (1968, §21.81).

The torque t_q on the cylinder, which is due only to the surface shear stress $\tau_0 = \mu\omega_0$, is given by

$$\begin{aligned}t_q &= a^2\oint\tau_0\,\mathrm{d}\theta \\ &= a^2\mu\oint\omega_0\,\mathrm{d}\theta\end{aligned} \tag{15}$$

and is in general non-zero. (Here $\oint$ denotes integration around the cylinder surface).

4. Forces from Riley's analysis

The forces and torque resulting from the analysis of Riley (1971) for uniform, circular, orbital flow are given below, taking terms to $O(\beta^{-\frac{1}{2}})$, and have been given in a different form by Chaplin (1984*b*).

The shear force f_s and the viscous component of pressure force f_p lead the velocity vector by $\frac{1}{4}\pi$ and have equal magnitudes:

$$f_s = f_p = 2\pi a^2 \rho U \omega \left(\frac{2K}{\pi R}\right)^{\frac{1}{2}}, \tag{16}$$

where ω is the angular orbital frequency and R is the Reynolds number ($= \beta K$).

Dividing by $\rho a U^2$ gives the non-dimensional force magnitude

$$F_s = F_p = \frac{2\sqrt{2(\pi)^{\frac{3}{2}}}}{K\beta^{\frac{1}{2}}}. \tag{17}$$

With $\beta = 483$
$$F_s = F_p = 0.7166/K \tag{18}$$

and total force
$$F = 1.4332/K. \tag{19}$$

Torque is divided by $\rho a^2 U^2$ and has a non-dimensional magnitude

$$T_q = \frac{4\pi^{\frac{1}{2}}}{\beta^{\frac{1}{2}}}. \tag{20}$$

With $\beta = 483$, $T_q = 0.3226$.

5. Results

We first consider the most idealized case of uniform, circular, orbital flow in detail. The sketch in figure 1 defines the force notation. We are concerned only with the viscous force, and in uniform orbital flow this may be obtained by subtracting $2\rho\pi a^2$ $\mathrm{d}\boldsymbol{u}/\mathrm{d}t$ from the total force vector. The force $\boldsymbol{F}_s$ due to shear stress is also output (and is part of the total viscous force $\boldsymbol{F}$).

The numerical parameters used in the computations are such that the forces, time-averaged over one cycle, are independent of further refinement of these parameters. Variations of force magnitude with time are shown in figure 2. The noise is due to the random walk used for simulating diffusion, and decreases as the number of vortices introduced is increased. Many cycles are computed (up to 20) and a periodic state appears to have been reached for $K \leqslant 1.5$ although not for $K = 2$. Around 100000 vortices are generated. The computer code automatically vectorizes on the Amdahl VP1200 and runs take up to 40 minutes CPU time. The shear force magnitude becomes steady much more quickly than that of the total viscous force. The time variations of the angle of the force vector relative to the onset velocity vector are shown in figure 3 and also reach a steady state quickly. Table 1 shows total viscous and shear force magnitudes and angles, averaged over the last five cycles computed, together with values from Riley's analysis. For $K = 0.1$, force magnitudes and angles are in close agreement with the theoretical analysis. Values of torque are also shown in table 1. Torque is a relatively small quantity and, for $K = 0.1$, figure 4 shows that the random noise is significant in relation to its mean value. For $K = 0.5$, the shear force magnitude and angle remain in close agreement with Riley's analysis, while the

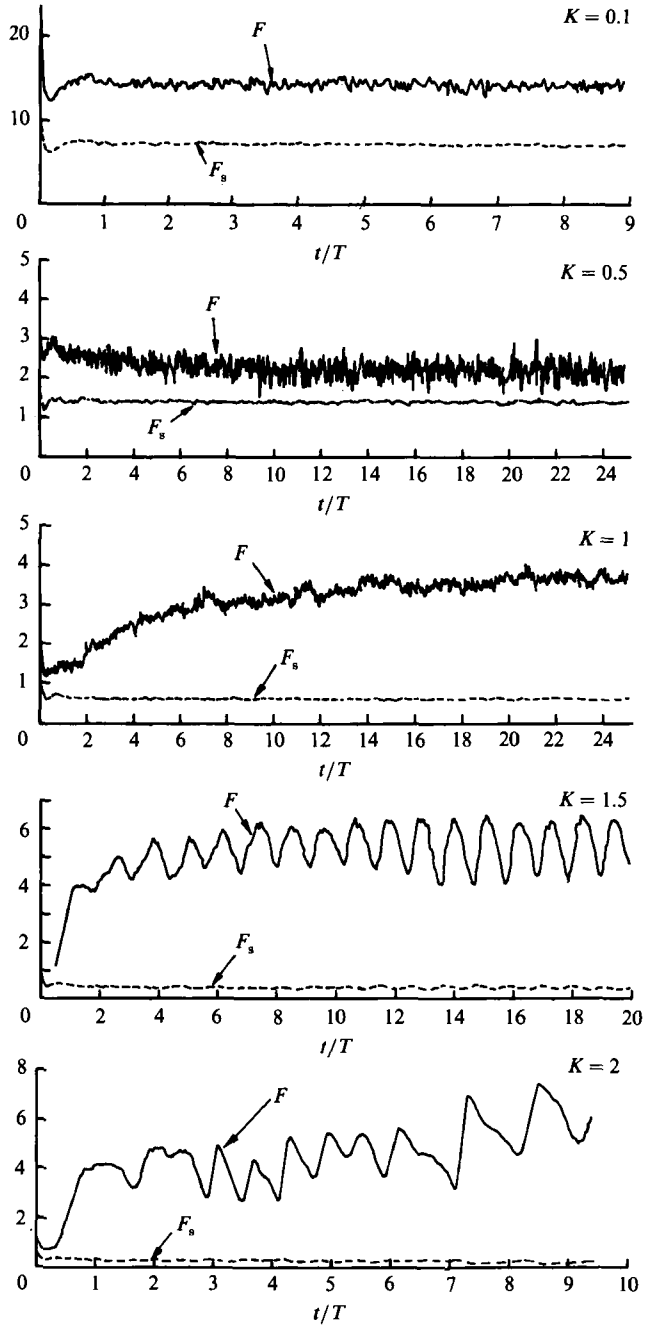

FIGURE 2. Variation of non-dimensional, viscous force magnitude F and shear force magnitude F_s with time in cycles, t/T, for $K = 0.1$, 0.5, 1, 1.5 and 2, with uniform, circular, onset flow.

total viscous force is approximately in the direction of the velocity vector. For $K = 1$, 1.5 and 2, the angle of the shear force remains close to that of Riley's analysis while its magnitude becomes increasingly less as K increases. The total viscous force is now predominantly in opposition to the acceleration vector, causing the reduction in the conventional inertia coefficient. With $K = 2$, a steady total viscous force

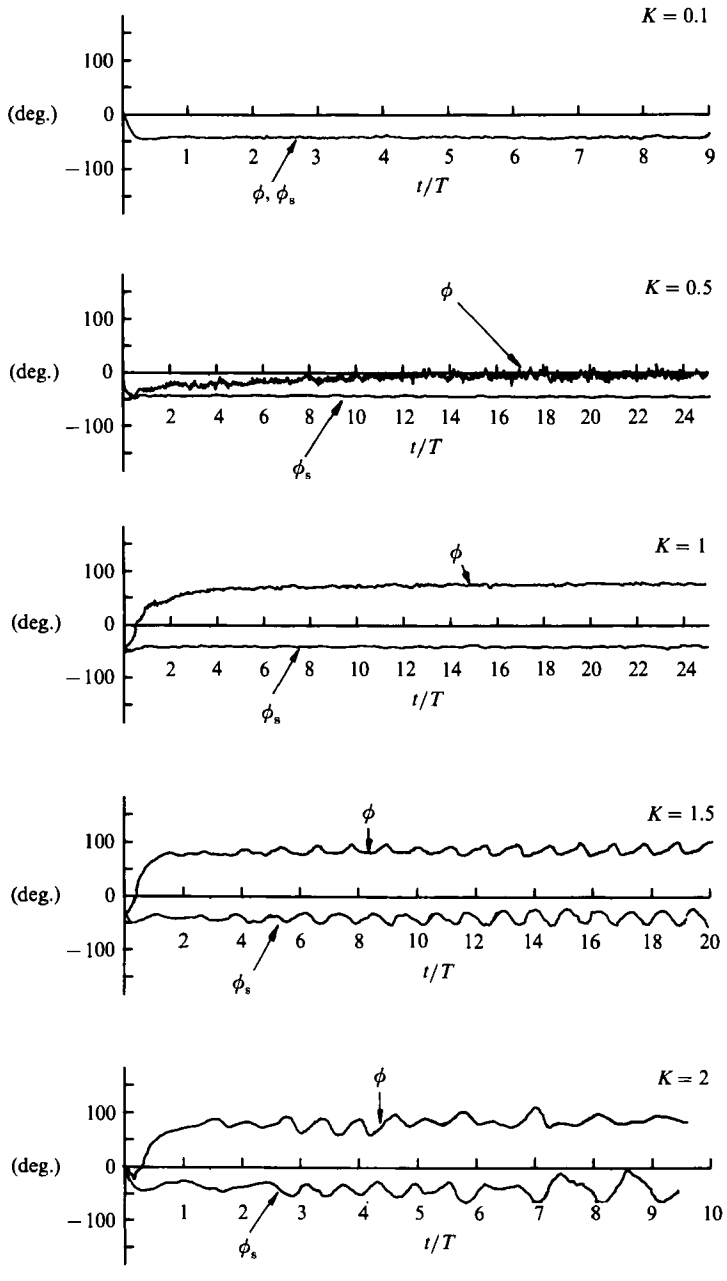

FIGURE 3. Variation of phase angle of viscous force and shear force relative to the velocity vector, ϕ and ϕ_s respectively, with time in cycles, t/T, for $K = 0.1$, 0.5, 1, 1.5 and 2, with uniform, circular, orbital, onset flow.

magnitude has clearly not been reached; vortex shedding is occurring and the flow structures are complex and unrepetitive. In view of this, the roughly constant angles for total viscous and shear force are perhaps surprising.

The flow structures for $K \leqslant 1.5$ are attached. Small 'separation bubbles' do occur with $K = 1.5$ and appear to produce the oscillations in the force and angle shown in figures 2 and 3. The term 'separation bubble' here indicates a region where the

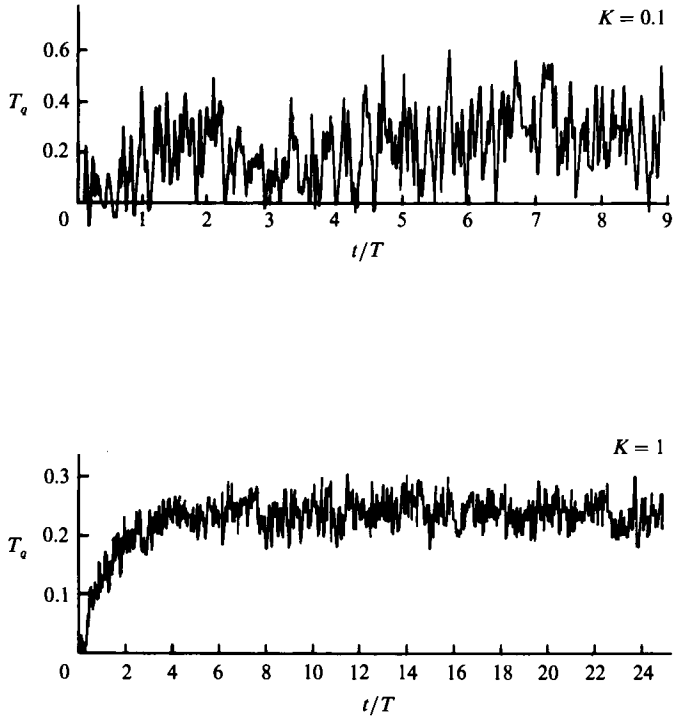

FIGURE 4. Variation of torque, T_q, with time in cycles, t/T, for $K = 0.1$ and 1, with uniform, circular, orbital, onset flow.

K	F	F_s	$\phi°$	$\phi_s°$	T_q	Half-cycles for averaging
0.1	14.87	7.22	−44	−43	0.28	11–18
	(14.34)	(7.17)	(−45)	(−45)	(0.32)	
0.5	2.20	1.40	−3	−43		41–50
	(2.87)	(1.43)	(−45)	(−45)		
1.0	3.68	0.58	76	−42	0.24	41–50
	(1.42)	(0.72)	(−45)	(−45)	(0.32)	
1.5	5.50	0.29	85	−39		31–40
	(0.95)	(0.48)	(−45)	(−45)		
2.0	5.20	0.19	86	−42		10–19
	(0.72)	(0.36)	(−45)	(−45)		

TABLE 1. For uniform, circular, orbital, onset flow: averaged total viscous and shear force magnitude, F and F_s; angle relative to the onset velocity vector, ϕ and ϕ_s; and torque, T_q, including, in parentheses, values from the analysis of Riley (1971).

surface streamline leaves the surface (bifurcates) and reattaches downstream to form a small 'bubble'. Examples are shown on the streamline plots close to the cylinder surface in figure 5 which indicates the intermittent nature of the bubbles. While separation in unsteady flow is not a well-defined phenomenon, these 'bubbles' have the appearance of separation bubbles associated with steady flow. Figures 6 and 7 (plates 1 and 2) show streamline and vorticity contours at various times for $K = 0.5$

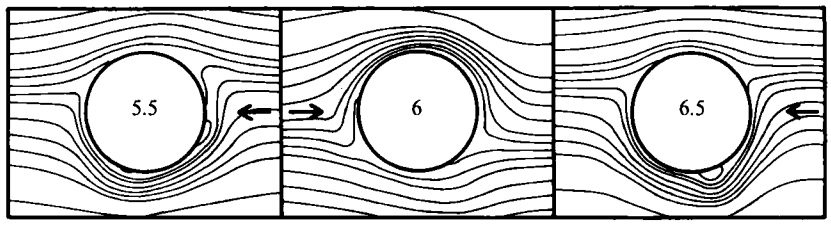

FIGURE 5. Streamline contours close to the cylinder surface in uniform, circular, onset flow with $K = 1.5$ at values of t/T shown by the number in the circle. The arrow indicates the onset flow direction.

and 1.5. Early and later times are shown to illustrate the initial development and the final structures. Vorticity contours enclose areas occupied by vorticity of clockwise and anticlockwise rotation, coloured green and red respectively. The magnitude on the contours at a given time is set arbitrarily to 10% of the average modulus of vorticity on the surface. It would appear that the small structures which eventually develop are a feature of the numerical method. Although they may resemble a transition phenomenon they occur at low Reynolds numbers when this would not be expected. In all cases, the centreline streamline is diverted around the cylinder in the direction of the orbital rotation, indicating that the tangential velocity near the cylinder has a phase lead over the outer flow velocity which is consistent with Stokes' oscillatory boundary-layer solution. For $K = 0.1$ (not shown), the vortical areas of each sense of rotation have a roughly similar shape. For $K = 0.5$, figure 6 shows that vorticity of one sense of rotation on the cylinder half-surface lagging the velocity vector remains close to the surface, while vorticity of opposite rotation wraps around the cylinder and outside the vorticity of opposite signed rotation. This effect is much more pronounced with $K = 1.5$, as shown in figure 7. On the lagging half-surface the outer vorticity reinforces the potential-flow velocity as the surface is approached. The no-slip condition generates the intense, oppositely signed vorticity close to the surface. The vorticity on the other side is weaker and the velocities smaller. In this way, the attached flow generates a force in opposition to the acceleration vector, while zero net circulation is maintained in the flow.

We now consider the total circulation Γ within a radial distance r' of the cylinder centre. The non-dimensional circulation Γ/aU, averaged over the last five cycles computed, is plotted against $r'/a-1$ in figure 8 for different values of K. The curves show the maximum circulation occurring at a radius which increases as K increases; their form may be related to the vorticity structures which have been described.

For the horizontal cylinder beneath waves, we consider case A in Chaplin (1984*b*), where the cylinder axis is 5 radii below mean water level, the depth parameter is 2.28 and linear wave theory is considered valid. The corresponding uniform, orbital flow is constructed by applying the onset velocities at the cylinder centre to the entire flow field. This gives an elliptical particle path with a ratio of horizontal to vertical axes of 1.094:1. To produce almost circular orbits, the depth parameter was increased to 10.0. We have thus considered four situations for $0 < K \leqslant 2$ and $\beta = 483$. In order of increasing complexity, these are:

I. Uniform, orbital flow with a circular, orbital path.
II. Uniform, orbital flow with an elliptical particle path with an axis ratio of 1.094:1.
III. Waves with a depth parameter of 10.0
IV. Waves with a depth parameter of 2.28.

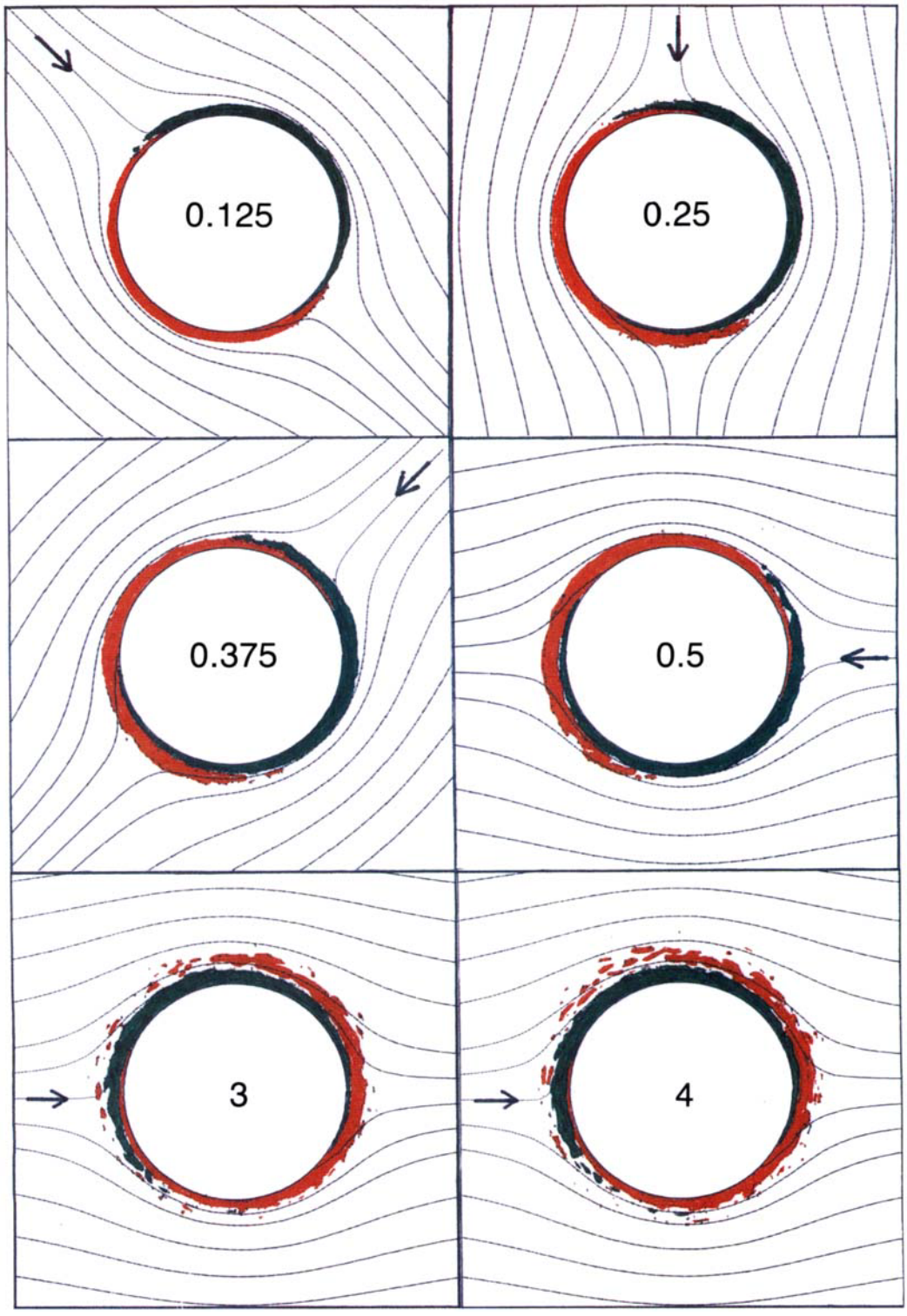

FIGURE 6. Streamline and vorticity contours for uniform, circular, onset flow with $K=0.5$ at various t/T, shown by the number in the cylinder. The arrow on the streamline shows the onset flow direction. The green area shows vorticity of clockwise rotation, the red area vorticity of anticlockwise rotation.

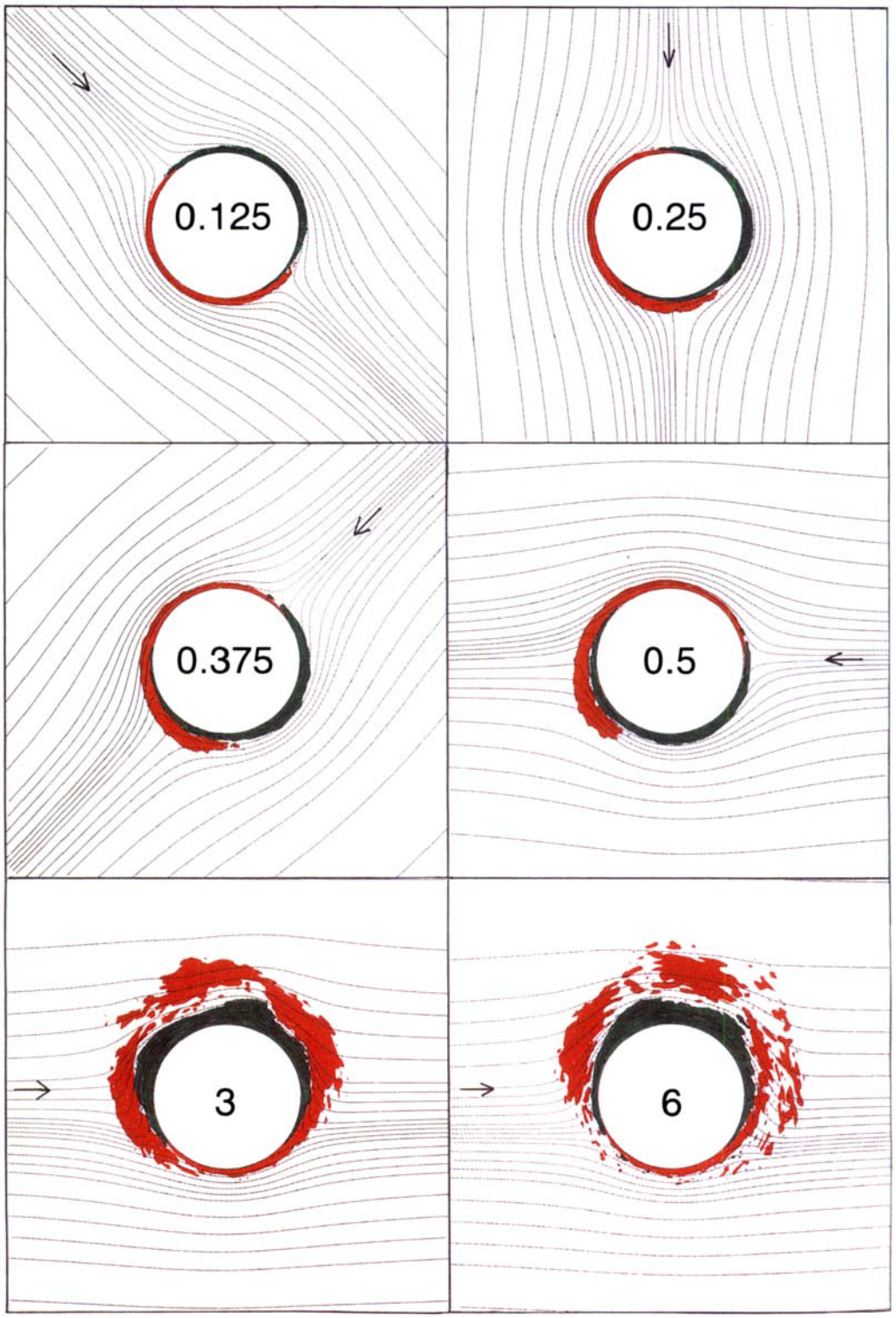

FIGURE 7. Streamline and vorticity contours for uniform, circular, onset flow with $K=1.5$, notation as figure 6.

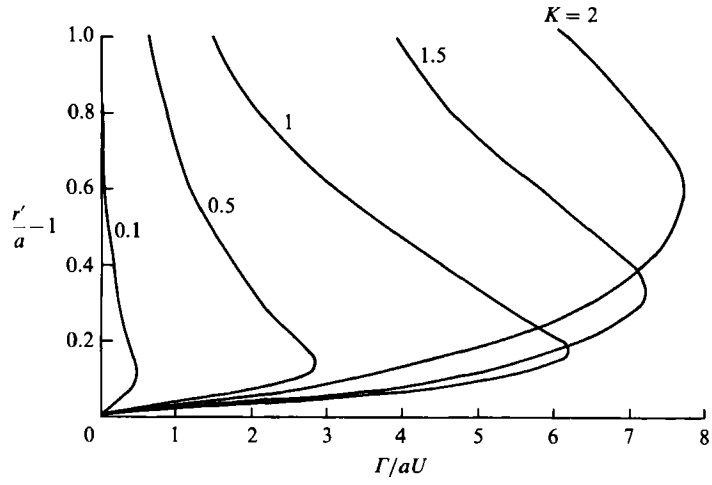

FIGURE 8. Variation of circulation Γ/Ua within a radial distance r' with $(r'/a-1)$ for $K = 0.1, 0.5, 1, 1.5$ and 2, averaged over the last five cycles computed, for uniform, circular, onset flow.

	Orbital Uniform Flow				Orbital Wave Flow			
	I		II		III		IV	
K	F	$\phi°$	F	$\phi°$	F	$\phi°$	F	$\phi°$
0.5	2.2	−3	2.1	−8	2.1	−1	2.0	−5
1.0	3.7	76	3.2	73	4.3	79	3.7	79
1.5	5.5	85	4.8	83	5.3	83	4.6	84
2.0	5.2*	86	5.4	86	2.6	33	2.5	41

TABLE 2. Viscous force magnitude F and angle ϕ relative to the onset velocity vector for situations I, II, III and IV, averaged over the last five cycles computed. (* Indicates steady state not reached.)

In waves, the calculation of potential-flow force must take account of non-uniform effects, e.g. Ogilvie (1963), in order to give the correct viscous force. These are particularly significant at the smaller K-values.

Viscous force variations for situations I, II, III and IV generally have a similar form and values of force magnitudes, and angles averaged over the last five cycles computed are given in table 2. It can be seen that there is a small influence of slight ellipticity and non-uniformity on force magnitude and angle for $K \leqslant 1.5$, while for $K = 2$ force magnitude and angle are quite different in uniform and wave flows. For the former, vortex shedding occurs with $K = 2$ while, for the latter, vortex shedding has started at the smaller value of $K = 1.5$.

The conventional inertia coefficient C_M is related to the viscous force magnitude F and angle ϕ by

$$C_M = 2 - K\overline{F\sin\phi}/\pi^2, \tag{21}$$

where the overbar indicates the time mean. Results from computations for situations I, II, III and IV are shown in figure 9, together with Case A of Chaplin with $\beta = 7600$. Results from computations for situation I with $\beta = 100$ were similar to those with $\beta = 483$ and in slightly closer agreement with the experiment at $\beta = 7600$.

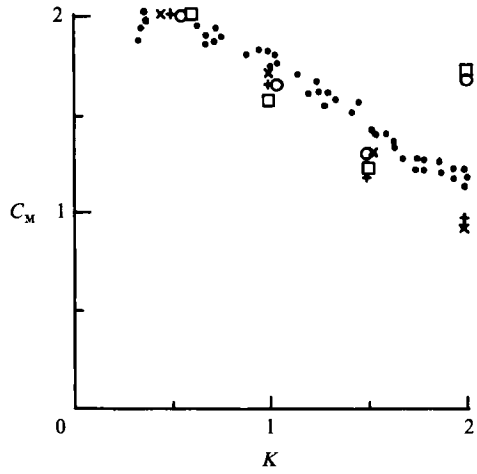

FIGURE 9. Variation of computed inertia coefficient C_M with K for situations I (+), II (×), III (□) and IV (○) with $\beta = 483$ and from experiments with $\beta = 7600$ (●).

6. Discussion and conclusions

It is interesting to compare results for uniform, orbital, onset flows with those for linear, oscillatory, onset flows, which have received much attention. In both cases, vortex shedding occurs for $K > 2$ and the flows are attached for $K < 1.5$. However, with orbital onset flows, Riley's analysis only gives a good viscous force prediction for very small K-values, e.g. 0.1 but not 0.5, while, for the linear case, Wang's analysis, using a similar technique, gives a reasonable prediction for $K < 2$. It should be mentioned that Wang's analysis includes terms up to $O(\beta^{-\frac{3}{2}})$, giving virtual identical forces to Stokes' analysis which includes terms up to $O(\beta^{-1})$. For orbital flow, the inclusion of terms of $O(\beta^{-1})$ in Riley's analysis reduces the viscous force magnitude by 1.3% and changes the phase by less than 1° (J. R. Chaplin, private communication). Although these higher-order terms in β produce only marginal changes, it is possible that, in the orbital case, theoretical analysis taken to arbitrarily high order in K and β would produce better force prediction.

The vorticity structures are quite different in the two situations, as might be expected. In linear, oscillatory flow, attached, periodic systems comprising pairs of weak vorticity regions are generated (Smith & Stansby 1991). The surface streamline bifurcates for a proportion of a half-cycle which decreases as K decreases. In orbital flows, such bifurcation was not apparent for $K \leqslant 1$ and only small 'separation bubbles' appeared with $K = 1.5$. For $0.5 \leqslant K \leqslant 1.5$, vorticity of one sense of rotation wraps itself all around the cylinder, outside a concentrated region of vorticity of oppositely signed rotation close to the half-surface of the cylinder lagging the onset velocity vector. This causes a viscous force in opposition to the acceleration vector, which results in the reduction in overall inertia coefficient. This reduction thus does not result from the concept of bound circulation associated with Riley's analysis. The computations require a large number of cycles to develop to an apparently periodic state and, since vorticity of one sense of rotation continues to wrap itself around the cylinder while diffusing away from the cylinder, it cannot be certain that the overall structures will maintain themselves indefinitely.

The numerical study has concentrated on the idealized case of uniform, circular orbital flows since it was shown that corresponding non-uniform orbital flows under

waves produced similar results, although separation and vortex shedding occurred at slightly lower K-values.

The original motivation for this study was provided by the results of experiments in waves which showed that the variation of C_M with K (for $K < 2$) was quite different from that for linear, oscillatory, onset flow. The β-values in the experiments were much higher than those used in the computations, which are limited to two-dimensional, laminar conditions. The experimental flows were almost certainly three-dimensional and turbulent but the variation of C_M with K has a similar form to the computed results, suggesting that the underlying flow phenomena are similar in the two cases.

The authors would like to acknowledge several useful discussions with Professor Chaplin. This work formed part of the research programme of the Marine Technology Directorate's Fluid Loading Programme, a programme of research jointly funded by the SERC, the Department of Energy and the offshore industry. The referees made a number of valuable comments.

REFERENCES

BEARMAN, P. W., DOWNIE, M. J., GRAHAM, J. M. R. & OBASAJU, E. 1985 Forces on cylinders in viscous oscillatory flows at low Keulegan–Carpenter numbers. *J. Fluid Mech.* **154**, 337.

CHAPLIN, J. R. 1984*a* Mass transport around a horizontal cylinder beneath waves. *J. Fluid Mech.* **140**, 175.

CHAPLIN, J. R. 1984*b* Nonlinear forces on a horizontal cylinder beneath waves. *J. Fluid Mech.* **147**, 449.

CHORIN, A. J. 1973 Numerical study of slightly viscous flow. *J. Fluid Mech.* **57**, 785.

CHORIN, A. J. 1978 Vortex sheet approximation of boundary layers. *J. Comput. Phys.* **27**, 428.

MILNE-THOMSON, L. M. 1968 *Theoretical Hydrodynamics*, 5th edn. Macmillan.

OGILVIE, T. F. 1963 First and second order forces on a cylinder submerged under a free surface. *J. Fluid Mech.* **16**, 451.

RILEY, N. 1971 Stirring of a viscous fluid. *Z. Angew. Math. Phys.* **29**, 439.

SARPKAYA, T. 1986 Force on a cylinder in viscous oscillatory at low Keulegan–Carpenter number. *J. Fluid Mech.* **165**, 61.

SMITH, P. A. 1986 Computation of viscous flows by the vortex method. Ph.D. thesis, University of Manchester.

SMITH, P. A. & STANSBY, P. K. 1988 Impulsively started flow around a circular cylinder by the vortex method. *J. Fluid Mech.* **194**, 45.

SMITH, P. A. & STANSBY, P. K. 1989 An efficient surface algorithm for random-particle simulation of vorticity and heat transport. *J. Comput. Phys.* **81**, 349.

SMITH, P. A. & STANSBY, P. K. 1991 Viscous oscillatory flows around cylindrical bodies at low Keulegan–Carpenter numbers using the vortex method. *J. Fluids Structures* (to appear).

STOKES, G. G. 1851 On the effect of the internal friction of fluids on the motion of a pendulum. *Trans. Camb. Phil. Soc.* **9**, 8.

WANG, C. Y. 1968 On high frequency oscillating viscous flows. *J. Fluid Mech.* **32**, 55.